Annales
Geophysicae

Variability and trend analysis of temperature and height in the upper troposphere and stratosphere region over the tropics (Réunion), by combining balloon-sonde and satellite measurements

Gregori de Arruda Moreira[1], Hassan Bencherif[2], Tristan Millet[2], and Damaris Kirsch Pinheiro[3]

[1]Federal Institute of Education, Science and Techonology of São Paulo (IFSP), São Paulo, 01109-010, Brazil
[2]Laboratoire de l'Atmosphère et des Cyclones, LACy, UMR 8105 CNRS, Université de La Réunion,
Météo-France, Reunion Island, France
[3]Federal University of Santa Maria, Santa Maria, 97105-900, Brazil

Correspondence: Gregori de Arruda Moreira (gregori.moreira@ifsp.edu.br)

Abstract. Tropopause height and temperature play a crucial role in atmospheric chemistry and radiative forcing and serve as key indicators of anthropogenic climate change. However, accurately determining this parameter requires advanced remote sensing techniques. This study compares tropopause height and temperature estimated from in-situ and remote sensing instruments (SHADOZ and COSMIC-1) with reanalysis data from MERRA-2 over Réunion from 2006 to 2020. The results reveal strong agreement between vertical temperature profiles obtained from SHADOZ and COSMIC-1, demonstrating that both can reliably estimate tropopause height using the Cold Point Temperature (CPT) and/or Lapse Rate Temperature (LRT) methods. Conversely, while MERRA-2 assimilates data from these sources, its fixed vertical resolution limits its ability to capture tropopause height variations accurately. Given the consistency between SHADOZ and COSMIC-1, their data were combined to construct a more refined dataset, which was then used to assess temperature trends. The analysis indicates a high influence of annual and semi-annual oscillations in Tropopause height dynamics, as well as, a decreasing trend in CPT and a slight increase in the Lapse Rate Tropopause (LRT) height.

1 Introduction

The troposphere is the atmospheric layer extending from the Earth's surface to around 18 km, depending on the latitude, so it is generally higher at the equator and decreases toward the poles. Inside this layer can be found the Tropical Tropopause Layer (TTL), which extends from 12–14 to 18 km, and it represents the transition region between the well-mixed convective troposphere and the radiatively controlled stratosphere (Fueglistaler et al., 2009; Randel and Jensen, 2013). The TTL is the main gateway for air to enter the stratosphere and a crucial indicator of anthropogenic climate change, as indicated by variations in the height and/or temperature of the tropopause (Santer et al., 2004).

The tropopause, found within the TTL, is a significant physical boundary that separates the unstable and moist troposphere from the stable and dry stratosphere. The temperature and height of such layer are influenced by both tropospheric and stratospheric forcing, like as changes in solar radiation (Reid and Gage, 1981), atmospheric angular momentum (Reid and Gage, 1984), El Niño-Southern Oscillation (ENSO), stratospheric ozone (Hoinka, 1998), Quasi-Biennal Oscillation (QBO) variability, explosive volcanic eruptions (Reid and Gage, 1985; Randel et al., 2000), and concentrations of Greenhouse Gases (GHG) (Zou et al., 2023). Consequently, tropospheric warming or stratospheric cooling can result in an increase in the tropopause height (Santer et al., 2004).

Traditional methods for sounding tropopause structure are usually based on in situ measurements (e.g., weather stations, radiosonde), model data (e.g., reanalysis data) and remote sensing (e.g., lidar, airborne, satellite soundings). The direct sounding technique usually has an uneven global distribution, with only sparse data distribution, especially in the southern hemisphere (Santer et al., 2004). On the other hand, reanalyses provide global and temporal coverage and a uniform data type (Xian and Homeyer, 2019). However, reanalyses suffer from coarser vertical resolution, which can render tropopause height detection unfeasible (Birner et al., 2006). Considering remote sensing, Global Navigational Satellite System Radio Occultation (GNSS-RO) stands out for offering accurate tropospheric profiles with high vertical resolution and global coverage independently of weather conditions. However, they are endowed with lower temporal resolution. Therefore, considering the limitations and advantages of each methodology, an option to improve the tropopause monitoring is to combine them. Although firstly it is necessary to identify their similarities and differences.

In this context, this study compares vertical temperature profiles from the Southern Additional Ozonesondes (SHADOZ) network, Constellation Observing System for Meteorology Ionosphere and Climate 1 (COSMIC-1), and Modern Era Retrospective analysis for Research and Applications – Version 2 (MERRA-2) over Réunion (2006–2020) to identify similarities and/or differences. Additionally, the study demonstrates how these datasets contribute to understanding variability in the Upper Troposphere–Lower Stratosphere (UT-LS) region. Finally, by combining ground-based balloon-sonde data and satellite-based COSMIC-1 observations, the variability and trend estimate of temperature in the tropical UT-LS region were investigated.

The paper structure is as follows: Sect. 2 gives a brief description of the experimental site and instruments used. The methodologies applied are presented in Sect. 3. The comparisons between temperatures and tropopause height estimated from SHADOZ, COSMIC-1 and MERRA-2 datasets are presented in Sect. 4. In Sect. 5, the results provided by the Trend-Run model are described. Finally, the conclusions are given in Sect. 6.

2 Materials

2.1 Study Area

Réunion (Fig. 1) is a volcanic island of the Indian Ocean with a population of $\sim 860\,000$ inhabitants. It covers around $2512\,\mathrm{km}^2$, and it is characterized by a humid tropical climate tempered by the oceanic influence of the trade winds blowing from the southeast. In addition, this climate is endowed with great variability, mainly due to the island landscape, which causes numerous microclimates (Britannica, 2025).
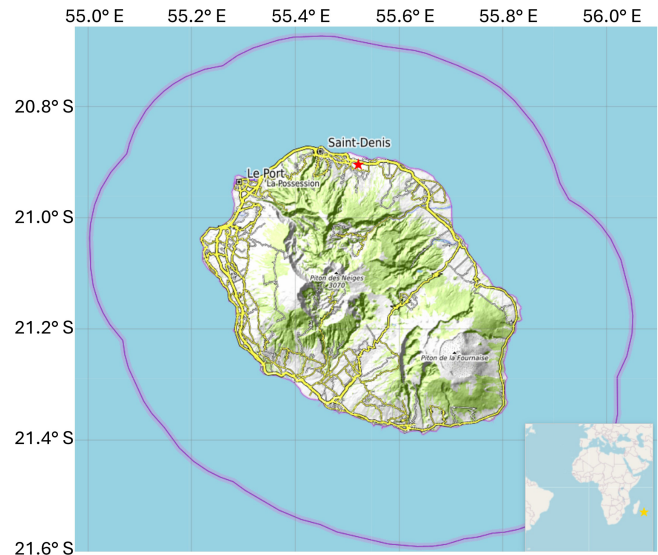
Figure 1. Geographical location of the study site, Réunion, a French overseas department in the southern tropics. The red star symbol indicates the measurement site where the balloon radiosondes are carried out, located to the north of the island at Roland Garros International Airport (20.9° S; 55.5° E).

2.2 Measurement by ballon-sonde experiment

Radiosonde measurements began in Réunion in 1993 (Baldy et al., 1996), and the station joined the Southern Hemisphere ADditional OZonesondes (SHADOZ) network in 1998, increasing the frequency of measurements to weekly. The SHADOZ network is a NASA project that aims to fill gaps in ozone observation in the southern tropics by increasing radiosonde frequencies at existing stations on a cost-sharing basis (Thompson et al., 2003). Each radiosonde is coupled in a balloon meteorological sonde, with an electrochemical cell (ECC) ozone-sonde, to transmit in-situ information on air pressure, temperature, relative humidity, and ozone partial pressure (Witte et al., 2017; Witte et al., 2018). The radiosonde technique has as its main disadvantages the limited spatial and temporal resolution, which can hinder a detailed observation of the dynamics of the tropopause. For this study, we used radiosonde temperature profiles from the study site (2006–2020), covering the COSMIC-1 mission's operational period and overlapping with its measurements. Radiosonde data can be accessed at the following link on the SHADOZ website (https://tropo.gsfc.nasa.gov/shadoz/Reunion.html, last access: 1 June 2024) (Sterling et al., 2018; Thompson et al., 2017; Thompson et al., 2021).

2.3 Temperature profiles from the COSMIC-1 experiment

The Constellation Observing System for Meteorology, Ionosphere, and Climate 1 (COSMIC-1) is a joint U.S.-Taiwanese program designed to provide advances in meteorology, iono-

spheric research, climatology, and space weather by using GNSS-RO, which is a satellite remote sensing technique that uses GNSS (e.g. Global Positioning System – GPS) measurements received by low-Earth orbiting satellites to profile the Earth's atmosphere and ionosphere with high vertical resolution and global coverage (Thompson et al., 2003; Anthes et al., 2008). The COSMIC-1 was launched into a circular low-Earth orbit on 15 April 2006, and retired in 2020. Its main limitation is the data gap during maintenance periods and after the beginning of the progressive degradation, which began in 2019 and resulted in total inoperability in May 2020. In this paper, we utilized all temperature profiles that have been provided by COSMIC-1 between 2006 and 2020. The profiles were selected for a specific geographic area, covering Réunion with a margin of $\pm 2°$ in latitude and $\pm 3°$ in longitude (UCAR COSMIC Program, 2002).

2.4 Temperature assimilation from the MERRA-2 reanalysis

The Modern-Era Retrospective Analysis for Research and Applications – Version 2 (MERRA-2) is a global atmospheric reanalysis produced by the National Aeronautics and Space Administration (NASA) Global Modeling and Assimilation Office (GMAO). MERRA-2 replaces the original MERRA so that more information is assimilated, such as modern hyperspectral radiance and microwave observations, along with GPS-Radio Occultation and NASA ozone datasets. Like COSMIC-1 time cover, we used vertical temperature profiles from MERRA-2 data from 2006 to 2020. Such temperature profiles can be obtained from the following MERRA-2 product, M2T3NVASM_5.12.4 (https://disc.gsfc.nasa.gov/datasets/M2T3NVASM_5.12.4/summary, last access: 1 June 2024), which is composed of 17 atmospheric variables and has a spatial resolution of $0.5° \times 0.625°$. All data are distributed on 72 pressure levels, ranging from 1000 to 0.01 hPa, with a time resolution of 3 h. These fixed heights can make it impossible to adequately observe some variations and trends in the tropopause behaviour (Zou et al., 2023). In this study, we used MERRA-2 average daily temperature profiles.

3 Methods

This study is based on the combination of 3 sources of temperature profile data at Réunion (radiosonde, COSMIC-1 and MERRA-2), over 15 years (2006–2020). Such a combination makes it possible to describe the thermal structure of the tropical atmosphere from the ground up to the mesosphere. However, given the differences in the methods of acquisition and production, the temperature data used may not offer the same uncertainties, or resolutions everywhere at all altitudes and in all seasons. The first step is to compare these datasets to each other and define the altitude ranges where

they can be used with confidence. Secondly, one could use all or a combination of these data to construct a coherent and regular time series, to investigate variability and temperature change in different atmospheric layers. Regarding the values obtained from the methods described in the following subsections, all reported uncertainties represent $\pm 2\sigma$ variability unless stated otherwise.

3.1 Cold-Point Tropopause

Based on thermal properties, it is possible to use the temperature profile to estimate the tropopause height from the Cold-Point Tropopause (TH_{CPT}), which can be defined as the height where the tropospheric temperature reaches its minimum value (Selkirk, 1993). In this paper, the temperature observed at this height z is denominated T_{CPT}. Such definition is given by the following equation:

$$T(z) \begin{cases} T_{CPT} = \min(T(z)) \\ TH_{CPT} = z, \\ \text{where } T(z) = T_{CPT} \end{cases} \quad (1)$$

3.2 Lapse-Rate Tropopause

From temperature profiles $T(z)$ it is possible to identify the tropopause height from the lowest level at which the lapse rate is less than $2\,K\,km^{-1}$ and it remains within this level for the next 2 km, such a point is denominated as the Lapse-Rate Tropopause (TH_{LRT}) (WMO, 1957), which is endowed of high stability, and signifies the thermodynamical transition between the troposphere and stratosphere. In this paper, the temperature detected at such height is denominated T_{LRT}. In addition, in all cases of the final time series where the criterium established in the previous paragraph was not identified, the TH_{LRT} was classified as NaN.

3.3 Stratopause Height

As defined by France et al. (2012), the stratopause is determined as the altitude where the stratospheric temperature reaches its maximum in the vicinity of 50 km. Therefore, considering the 3 databases applied in this study, only the COSMIC-1 temperature profiles can be used to detect the stratopause, due to their vertical range and resolution.

3.4 Forcings parametrization in the Trend-Run model

The Trend-Run model, a multiple linear regression model, was first adapted at the University of Réunion to analyse temperature trends in the southern subtropical upper troposphere-lower stratosphere (UT-LS) (Bencherif et al., 2006). This model decomposes the variations of a time-series signal, $S(t)$, into components representing atmospheric forcings:

$$S(t) = c_1 SAO(t) + c_2 AO(t) + c_3 QBO(t)$$
$$+ c_4 ENSO(t) + c_5 SSN(t) + c_6 IOD(t) + \varepsilon \quad (2)$$

where ε represents the residuals term which includes the trend, and c_i (i ranging from 1 to 6) are contribution coefficients of the respective forcings. The coefficients c_i can be derived using the least-squares method, which minimizes the residual variance, while the trend is parameterized as linear: $\text{Trend}(t) = a_0 + a_1 t$, where a_0 is a constant, and a_1 is the trend slope. The initial model incorporated key forcings, including annual and semi-annual oscillations (AO, SAO), quasi-biennial oscillation (QBO), El Niño-Southern Oscillation (ENSO), sunspot numbers (SSN), AO and SAO represent seasonal cycles, with SAO being particularly dominant in the tropics above 35 km altitude. SAO amplitudes decrease with latitude but can intensify in the subtropics, depending on altitude. QBO is parametrised as a proxy of the zonal wind at 70 hPa derived from balloon measurements at the Equator (Singapore), while the ENSO is parametrized with the Multivariate ENSO Index (Randel and Cobb, 1994). The model was further extended by Bègue et al. (2010) to include the Indian Ocean Dipole (IOD), which describes sea surface temperature (SST) anomalies in the Indian Ocean's east-west dipole (Saji et al., 1999; Morioka et al., 2010). The IOD, measured by the Dipole Mode Index (DMI), quantifies the SST difference between the western (50–70° E, 10° S–10° N) and eastern (90–110° E, 10° S–Equator) Indian Ocean (Sivakumar et al., 2017). The DMI data were sourced from the Japanese Agency for Marine-Earth Science and Technology. The model's performance, measured with the coefficient of determination (R^2), evaluates its ability to explain how much the forcings explain the signal variability. Decadal temperature trends (in Kelvin) were calculated to evaluate long-term changes. For details on the Trend-Run model and its parameterizations, see Bencherif et al. (2006) and Bègue et al. (2010).

4   Analysis of temperature profiles

In this section, a comparison is performed among the vertical temperature profiles provided by MERRA-2 ($T_{\text{MERRA-2}}(z)$), SHADOZ ($T_{\text{SHADOZ}}(z)$) and COSMIC-1 ($T_{\text{COSMIC-1}}(z)$), The limitations and advantages of each system will be presented and then a database will be created combining the data from the instruments that are endowed of the most similar profiles.

4.1   Day-to-day Comparisons

Figure 2 shows daily comparisons of vertical temperature profiles from SHADOZ ($T_{\text{SHADOZ}}(z)$), COSMIC-1 ($T_{\text{COSMIC-1}}(z)$), and MERRA-2 ($T_{\text{MERRA-2}}(z)$) for three selected dates: 25 June 2014 (Fig. 2a), 19 November 2014 (Fig. 2b), and 17 September 2014 (Fig. 2c). The corresponding temperature differences (SHADOZ – COSMIC-1 and SHADOZ – MERRA-2) for the same dates are presented in Fig. 2d, e, and f.
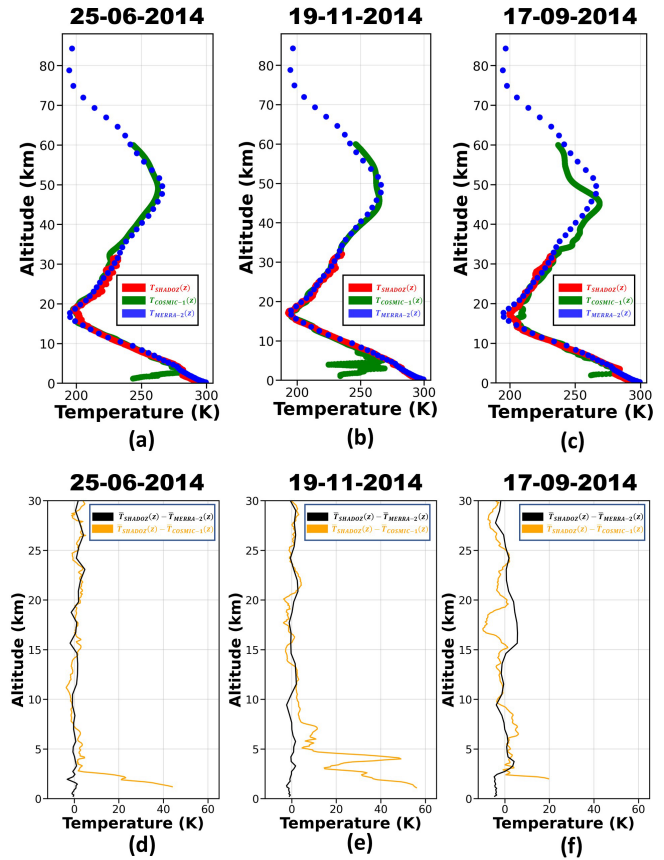
Figure 2. Comparison between $T_{\text{SHADOZ}}(z)$ (red), $T_{\text{COSMIC-1}}(z)$ (green) and $T_{\text{MERRA-2}}(z)$ (blue) profiles on 25 June 2014 **(a)**, 19 November 2014 **(b)** and 17 September 2014 **(c)** and the difference between $T_{\text{SHADOZ}}(z)$ and $T_{\text{COSMIC-1}}(z)$ (orange line) and $T_{\text{SHADOZ}}(z)$ and $T_{\text{MERRA-2}}(z)$ (black line) profiles to the same days **(d)**, **(e)**, and **(f)**, respectively.

On 25 June and 19 November, the difference between $T_{\text{SHADOZ}}(z)$ and $T_{\text{MERRA-2}}(z)$ does not exceed 4.0 K, so that the minimal differences are observed below 6.0 km and in the region between 16.0 and 18.0 km. On the other hand, $T_{\text{SHADOZ}}(z)$ and $T_{\text{COSMIC-1}}(z)$ present a significant difference below 5.0 km (in some points the difference is higher than 40.0 K). However, above 10.0 km, on both days, $T_{\text{SHADOZ}}(z)$ and $T_{\text{COSMIC-1}}(z)$ are very similar, so that the difference does not exceed 5.0 K.

On 17 September, $T_{\text{SHADOZ}}(z)$ and $T_{\text{MERRA-2}}(z)$ present a difference lower than 5.0 K in the region below 15.0 km. Above 15.0 km, the difference increases significantly, mainly in the region between 15.0 and 20.0 km. As observed in the other two days, the higher difference between $T_{\text{SHADOZ}}(z)$ and $T_{\text{COSMIC-1}}(z)$ is observed in the first 5.0 km. However, a significant difference (around 6 K) also is observed in the region between 15.0 and 20.0 km, resulting in a variation of approximately 2.1 km between the CPT estimated by $T_{\text{SHADOZ}}(z)$ (17.3 km) and $T_{\text{COSMIC-1}}(z)$ (15.2 km). In ad-

dition, a difference between $T_{COSMIC-1}(z)$ and $T_{MERRA-2}(z)$ in the region above 30.0 km is significantly higher than that observed in previous analyses. However, as will be demonstrated in the next sections, it is possible to consider 17 September as an exceptional case, where $T_{COSMIC-1}(z)$ presents an abnormal behavior.

4.2 Weekly (SHADOZ) and daily (COSMIC-1) temperature profiles

Figure 3 presents the curtain plot from the ground up to 30.0 km of weekly temperature profiles as measured by balloon-sondes (T_{SHADOZ}) at Réunion from 2006 to 2020. The figure shows that during this period, balloon-sonde measurements at Réunion were carried out almost continuously, at the rate of one release per week, except in 2007, due to a shortage of stock supplies, which resulted in a 3-month interruption. For each profile, the tropopause height was determined and corresponds to the location of the LRT (LRT$_{SHADOZ}$) and CPT (CPT$_{SHADOZ}$), as defined above. Their respective positions are superimposed in Figure 3 by grey and black dots. Overall, the altitude of the CPT$_{SHADOZ}$ varies between 16.0 and 19.0 km, with an average position of [17.2 ± 1.4] km, while the LRT$_{SHADOZ}$ varies between 14.0 and 16.0 km, with an average value of [14.9 ± 1.5] km, resulting in an average difference of [2.3 ± 0.3] between CPT$_{SHADOZ}$ and LRT$_{SHADOZ}$. The range of CPT$_{SHADOZ}$ values agrees with the results reported by Bègue et al. (2010), and with the average value obtained by Sivakumar et al. (2006) [17.2 ± (1σ) 0.6] km. On the other hand, the LRT$_{SHADOZ}$ range is below of Bègue et al. (2010) results, as well as the average value is lower than that one reported by Sivakumar et al. (2006) [16.0 ± (1σ) 0.7] km. Consequently, the average difference between CPT$_{SHADOZ}$ and LRT$_{SHADOZ}$ is higher than the values obtained by Bègue et al. (2010), Sivakumar et al. (2006), and Zhran et al. (2023) [0.91 ± (1σ) 0.15] km, [1.09 ± (1σ) 0.94] km, and 0.92 km, respectively. It is important to highlight that the number of LRT$_{SHADOZ}$ cases are lower than those of CPT$_{SHADOZ}$, as not all $T_{SHADOZ}(z)$ profiles have the essential characteristics for calculating the LRT.

Similar to Fig. 3, Fig. 4 presents the curtain plot of the vertical temperature profiles from the surface to 60.0 km height, as derived from daily COSMIC-1 measurements from 2006 to 2020. By comparison to SHADOZ temperature profiles, COSMIC-1 profiles present a higher vertical range, up to the mesosphere (limited here to 60.0 km) with greater temporal sampling. Table 1 presents the total number of temperature profiles per month used in the present study from SHADOZ and COSMIC-1 measurements. COSMIC-1 presents a lack of data in February and March 2014, and from June to December 2019. In addition, based on the density of CPT and LRT points in Figure 4, it can be noted that there was a decrease in the number of COSMIC-1 overpasses over the study site from 2017.
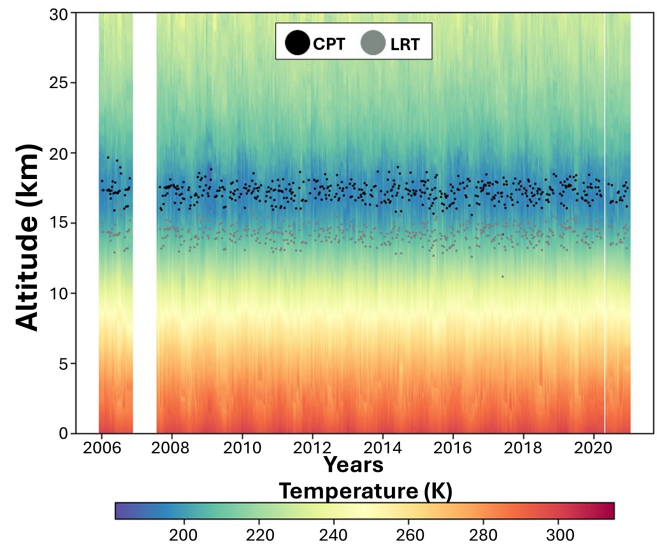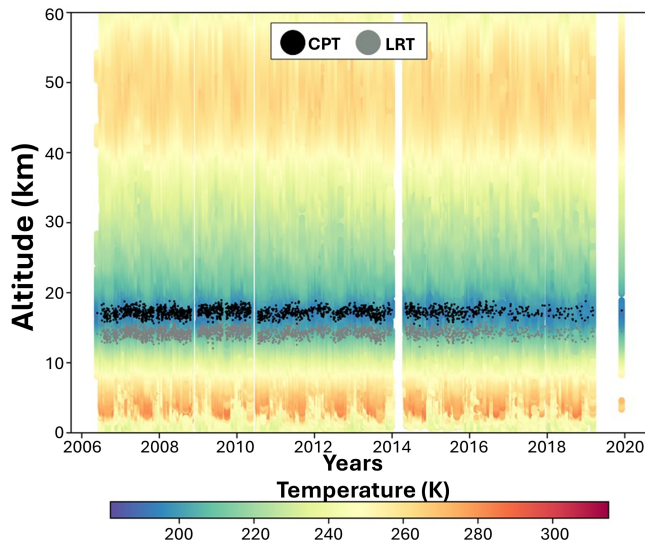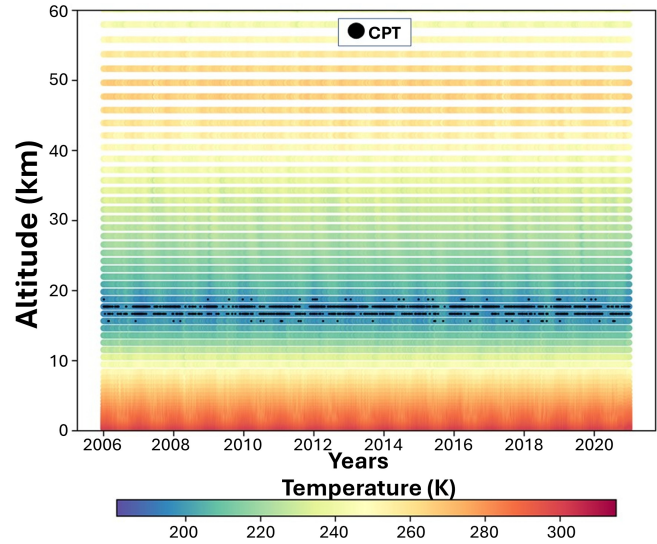

Figure 3. Time-height temperature cross-section over Réunion from weekly balloon-sonde profiles from January 2006 to December 2020. Black and gray dots indicate the CPT and LRT heights, respectively.

A quick visual comparison of the T_{SHADOZ} (Fig. 3) and the $T_{COSMIC-1}$ (Fig. 4) shows significant differences below 10 km altitude. The CPT values obtained from COSMIC-1 data (CPT$_{COSMIC-1}$) are located in the same range of CPT$_{SHADOZ}$, so that the average value provided by COSMIC-1 data [17.2 ± 1.3] km is similar to average CPT$_{SHADOZ}$ ([17.2 ± 1.4] km) and almost identical to the value obtained by Sivakumar et al. (2006). Regarding the LRT (LRT$_{COSMIC-1}$, the range of values [between 14.0 and 16.0 km] and the average value ([14.7 ± 1.2] km) are similar to that one obtained from SHADOZ data, consequently the average difference between CPT$_{COSMIC-1}$ and LRT$_{COSMIC-1}$ [2.9 ± 1.9] km is similar to that one observed between the SHADOZ data. These results agree with those presented by Xia et al. (2021), who found an average difference of 2.67 km between CPT$_{COSMIC-1}$ and LRT$_{COSMIC-1}$.

In contrast to SHADOZ and COSMIC-1 data, MERRA-2 does not show any data gap (Fig. 5). Although the $T_{MERRA-2}$ have a reasonable agreement with T_{SHADOZ} and $T_{COSMIC-1}$ in tropopause region (Fig. 2), MERRA-2 data cannot be used to detect the tropopause height accurately, because the heights are fixed, as mentioned previously, then the results obtained have low variability, making it impossible to observe the variations and trends in this layer (Fig. 5). Zou et al. (2023), when comparing CPT and LRT values using different reanalysis databases (ERA-Interim, MERRA-2 and NCEP/NCAR Reanalysis 1), also address the difficulty of refinement due to the coarser vertical resolution.

Table 1. Total monthly number of temperature profiles used from SHADOZ and COSMIC-1 measurements at the Réunion site.

	JAN	FEB	MAR	APR	MAY	JUN	JUL	AUG	SEP	OCT	NOV	DEC	Total
SHADOZ	40	43	46	46	45	53	30	24	54	48	43	32	504
COSMIC-1	159	163	197	175	158	169	223	216	162	164	112	99	1997

Figure 4. Same as Fig. 3 but concerning COSMIC-1 measurements over Réunion.

Figure 5. Time-height temperature cross-section over Réunion from daily MERRA-2 data from January 2006 to December 2020. The black dots indicate the CPT.

4.3 Global Comparison

In this subsection, the global mean temperature profiles obtained from the 3 datasets (SHADOZ, COSMIC-1 and MERRA-2) were computed and compared with each other. A global temperature profile is obtained by averaging all the temperature profiles recorded by the same experiment over the entire study period (2006–2020). We thus obtained 3 global average profiles for the 3 datasets: $\overline{T}_{\mathrm{SHADOZ}}(z)$, $\overline{T}_{\mathrm{COSMIC\text{-}1}}(z)$, and $\overline{T}_{\mathrm{MERRA\text{-}2}}(z)$. They are superimposed in Fig. 6a, respectively in red, green and blue dots. Figure 6b shows the temperature differences in the 0.0–30.0 km altitude range between the COSMIC-1 and MERRA-2 global profiles and the SHADOZ global profile: $\left(\overline{T}_{\mathrm{SHADOZ}}(z) - \overline{T}_{\mathrm{COSMIC\text{-}1}}(z)\right)$ and $\left(\overline{T}_{\mathrm{SHADOZ}}(z) - \overline{T}_{\mathrm{MERRA\text{-}2}}(z)\right)$, respectively in orange and black lines. Using SHADOZ data as a reference, it is evident that COSMIC-1 temperature values progressively overestimate as height decreases below 8.0 km, whereas MERRA-2 assimilated temperatures show excellent agreement. The largest differences are obtained between SHADOZ and COSMIC-1 values in the lower troposphere, up to 55.0 K near the surface (see Fig. 6b).

Above 10.0 km, the differences between $\overline{T}_{\mathrm{COSMIC\text{-}1}}$ and $\overline{T}_{\mathrm{SHADOZ}}$ reach approximately 1.0 K, continuing in this way until the end of the $\overline{T}_{\mathrm{SHADOZ}}$ profile (around 30.0 km).

$\overline{T}_{\mathrm{MERRA\text{-}2}}$ appears as a combination between $\overline{T}_{\mathrm{SHADOZ}}$ and $\overline{T}_{\mathrm{COSMIC\text{-}1}}$, following the behavior of SHADOZ in the first 30.0 km, so that the average profiles do not present a difference greater than 2.0 K, and follows COSMIC-1 in the rest of the profile. Such behavior was also observed by Tegtmeier et al. (2020). The similarity of $T_{\mathrm{MERRA\text{-}2}}$ with T_{SHADOZ} and $T_{\mathrm{COSMIC\text{-}1}}$ is justified by the composition of the MERRA-2 reanalysis data, since in addition to being based on balloon-sonde profiles, these reanalysis data incorporate GPS-Radio Occultation information, which did not happen with the original MERRA data.

4.4 Seasonal Comparison

As reported by several authors (Seidel et al., 2001; Bencherif et al., 2006; Sivakumar et al., 2011a; Bègue et al., 2010; Shangguan and Wang, 2022; Zhran and Mousa., 2023), the thermal structure of the atmosphere is seasonally dependent, notably in the tropics and subtropics. Thus, we examined and compared temperature profiles averaged by season (summer -DJF, autumn -MAM, winter -JJA and spring -SON). Plots in the upper panel of Fig. 7a–d superimpose the seasonal temperature profiles obtained from SHADOZ, COSMIC-1 and MERRA-2 and the associated seasonal temperature differ-
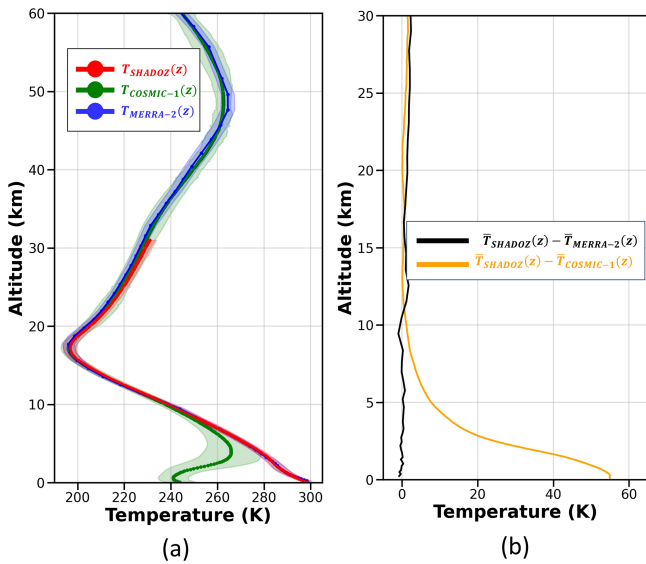
Figure 6. (a) Global average temperature profiles over Réunion site from SHADOZ (red line), COSMIC-1 (green line) and MERRA-2 (blue line), framed with their $\pm 2\sigma$ (standard deviation) profiles (in coloured shadows). **(b)** Difference profiles: $\left(\overline{T}_{\text{SHADOZ}} - \overline{T}_{\text{MERRA-2}}\right)$ and $\left(\overline{T}_{\text{SHADOZ}} - \overline{T}_{\text{COSMIC-1}}\right)$, respectively in black and orange lines.

ences with the SHADOZ data as a reference (plots of the lower panel of Fig. 7e–h).

The altitude range of agreement between the seasonal $\overline{T}_{\text{SHADOZ}}$ and $\overline{T}_{\text{COSMIC-1}}$ temperature profiles vary depending on the season, as indicated in Fig. 7b. To enable comparison between different seasons, a horizontal dashed line is added to the temperature difference profiles. This line shows the altitude at which the temperature difference between $\overline{T}_{\text{SHADOZ}}$ and $\overline{T}_{\text{COSMIC-1}}$ begins to be lower than 5 %. It appears from this line that the altitude of validity of the COSMIC-1 measurements depends on the season. It is possible to identify a seasonal behavior, where the highest limit occurs in summer (5.3 km), then it decreases continuously, reaching 4.3 km in Autumn, and the lowest value in winter and spring (2.8 km). The best agreement between $\overline{T}_{\text{SHADOZ}}$ and $\overline{T}_{\text{COSMIC-1}}$ values are observed during the dry season (JJA), while during the wet season (DJF) $\overline{T}_{\text{COSMIC-1}}$ profiles seem to underestimate the $\overline{T}_{\text{SHADOZ}}$ values over the widest range of altitudes. On the other hand, the difference between $\overline{T}_{\text{SHADOZ}}$ and $\overline{T}_{\text{MERRA-2}}$ does not present a seasonality. During all seasons, the differences do not exceed 3.0 K. The higher values are observed between 11.0 and 14.0 km, and above 19.0 km. In these regions difference between $\overline{T}_{\text{SHADOZ}}$ and $\overline{T}_{\text{MERRA-2}}$ is higher than that one observed between $\overline{T}_{\text{SHADOZ}}$ and $\overline{T}_{\text{COSMIC-1}}$.

The CPT values estimated by both databases are quite similar, so that when considering the uncertainty values, it can be stated that the seasonal values obtained from COSMIC-1 and SHADOZ are practically coincident. The $\text{CPT}_{\text{COSMIC-1}}$

sometimes overestimates and at others underestimates the $\text{CPT}_{\text{SHADOZ}}$. The lower absolute difference between them is observed during the Winter (26 m), and the higher one in Autumn (122 m). The average $\text{CPT}_{\text{SHADOZ}}$ has a seasonal behavior similar to that one observed by Seidel et al. (2001), where the maximum and minimum values were observed in Summer and Winter, respectively. Bègue et al. (2010) also identified the maximum $\text{CPT}_{\text{SHADOZ}}$ during the summer, as well as Astudillo et al. (2020) using Ground-Based GNSS Observations and Schmidt et al. (2004) using GPS RO data from the German CHAMP (CHAllenging Minisatellite Payload) satellite mission. This seasonal tropopause behavior also was observed by Sivakumar et al. (2011a), which identified the minimum $\text{CPT}_{\text{SHADOZ}}$ during the winter, and Zhran and Mousa (2023). On the other hand, although the lowest values of $\text{CPT}_{\text{COSMIC-1}}$ occur during winter, in agreement with the results obtained by Seidel et al. (2001) and Sivakumar et al. (2011a), the maximum values occur in autumn, what is not in agreement with the current literature. It is important to highlight that this seasonal behaviour reinforces the influence of solar radiation in tropopause height, mainly in tropical and subtropical regions (Sivakumar et al., 2011a).

Regarding the $\text{CPT}_{\text{SHADOZ}}$ temperature, the average monthly values obtained are similar, although a little bit smaller than those estimated by Bègue et al. (2010), so that the lower and higher mean absolute difference are -0.1 K (February, the coldest month identified by Bègue et al., 2010) and -1.5 K (September, the hottest month identified by Bègue et al., 2010), respectively. In this work the coldest month is January ($[193.1 \pm 4.6]$ K) and the hottest is October ($[197.1 \pm 4.6]$ K). Considering $\text{CPT}_{\text{COSMIC-1}}$, excepting May, where the average $\text{CPT}_{\text{COSMIC-1}}$ is 2.7 K higher than the $\text{CPT}_{\text{SHADOZ}}$ obtained by Bègue et al. (2010), all other months have a smaller average temperature value, so that the lower and higher absolute difference are -0.3 (August) and -2.7 (April), respectively. The coldest and the hottest month are February ($[192.1 \pm 4.6]$ K) and September ($[197.5 \pm 4.8]$ K), as observed by Bègue et al. (2010), respectively.

Due to the necessity of data above 40 km, only $T_{\text{COSMIC-1}}$ was applied to estimate the stratopause height, as indicated previously in Sect. 3.3. The stratopause appears to be highest in spring ($[48.9 \pm 4.6]$ km) with a maximum temperature of $[266.3 \pm 0.4]$ K, whereas it is lowest in summer ($[48.5 \pm 4.2]$ km) with a temperature maximum of around $[267.2 \pm 0.8]$ K. These results agree with the outcomes of other studies conducted at tropical locations. Batista et al. (2009) analyzed 14 years (from 1993 to 2006) of temperature profiles recorded by a sodium resonance LiDAR at São José dos Campos, Brazil (23° S, 46° W). They found that the local stratopause altitude was $\sim$ 49 km, with the maximum temperature varying from 265 to 270 K. Moreover, Sivakumar et al. (2011b) used temperature profiles over Réunion recorded between 1994 and 2007 by a Rayleigh LiDAR and reported that the stratopause height occurrence
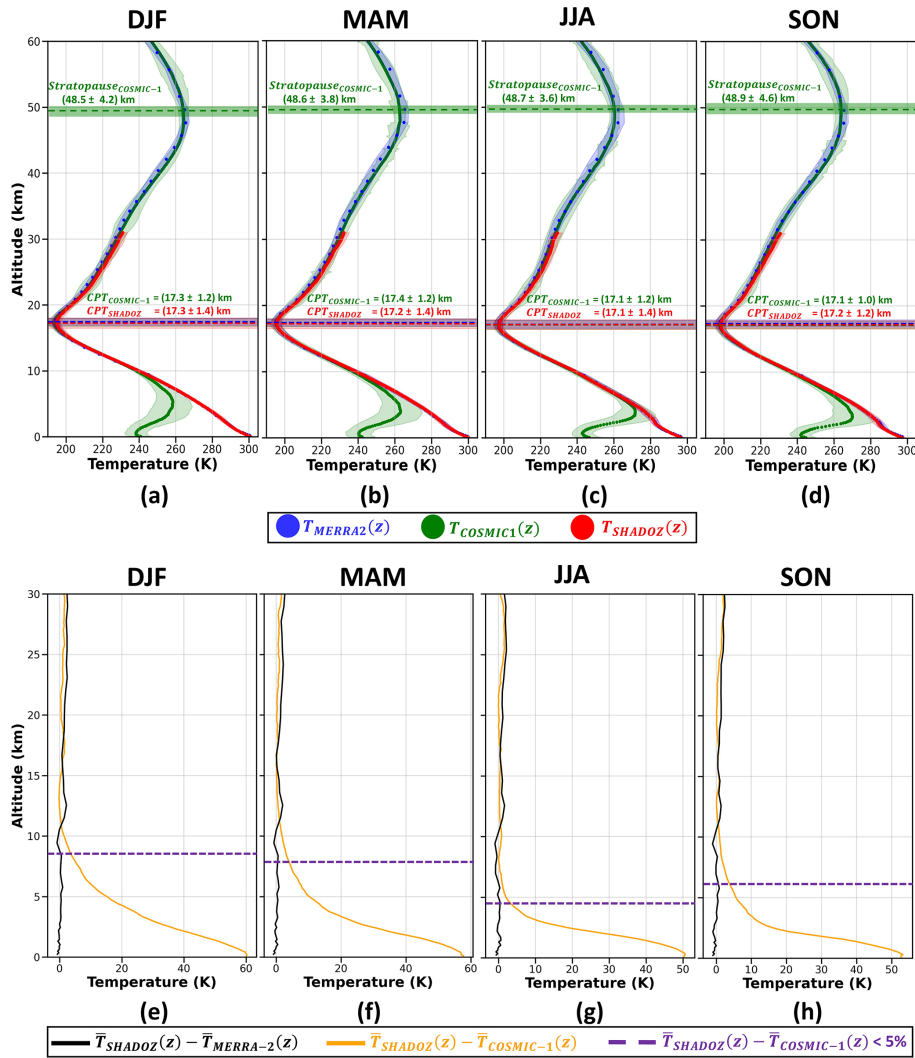
Figure 7. In the upper part is presented a seasonal comparison (**a** DJF, **b** MAM, **c** JJA, and **d** SON) among $T_{\text{SHADOZ}}(z)$ (red), $T_{\text{COSMIC1}}(z)$ (green) and $T_{\text{MERRA-2}}(z)$ (blue) profiles, and their respective standard-deviations. In the lower part is presented a seasonal comparison (**e** DJF, **f** MAM, **g** JJA, and **h** SON) among the differences of $T_{\text{SHADOZ}}(z)$ and $T_{\text{MERRA-2}}(z)$ (black line) and $T_{\text{SHADOZ}}(z)$ and $T_{\text{COSMIC-1}}(z)$ (orange line). The dotted purple line represents the height where the difference between $T_{\text{SHADOZ}}(z)$ and $T_{\text{MERRA-2}}(z)$ is lower than 5 %.

was in the 47–49 km height range, with temperatures ranging from 260 to 270 K. In addition, the same seasonal behaviour of the stratopause height presented in Fig. 6 was observed by France et al. (2012) and Vignon and Mitchell (2015) in their climatology studies using the Microwave Limb Sounder (MLS) and reanalysis data (MERRA-2).

4.5 Combination between SHADOZ and COSMIC-1 datasets

Considering the results presented in the previous section, where SHADOZ and COSMIC-1 temperature profiles showed a good agreement in the 10–28 km altitude range, we merged the two datasets to construct quasi-continuous and regular space-by-time matrix temperature values. SHADOZ

and COSMIC-1 have different temporal resolutions (1 profile per week and 1 profile every 2 d, respectively), as mentioned in Sect. 4.2. Therefore, the final database was created from the combination of these two datasets, and for days where there is data from both instruments, only the SHADOZ data were considered. Then, the daily temperature series obtained were reduced to monthly and kilometric averages and are presented in Fig. 8. This new dataset will be applied in the trend analyses (Sect. 5).

5 Trend Model Analysis

For trend analysis, we used the multiple linear regression method taking into account the same *forcings* used by Bègue et al. (2010) and by Toihir et al. (2018): annual and
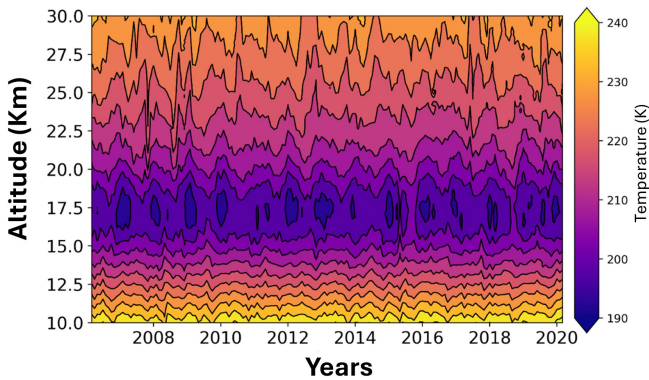
Figure 8. Monthly time-height temperature cross-section over Réunion constructed by combining SHADOZ and COSMIC-1 profiles.

semi-annual cycles, quasi-biennial oscillation, and ENSO (Sect. 3.4).

The analysis of the R^2 profile, as depicted in Fig.8a, reveals two layers where the Trend-Run model performs well and explains more than 65% of the temperature variability: one layer at around 10 km and another at around 18 km. Additionally, the R^2 profile shows two minima ($\sim 40\%$), where the Trend-Run model performs less well, in the upper troposphere (14 km) and the upper stratosphere (26–27 km). This result is not surprising given the short length of the time series (2006–2020). We then examine temperature trends in two tropospheric heights (10 and 15 km) and two stratospheric layers (19 and 24 km), in addition to temperature trends at the local tropopause. Figure 8b overlays the profiles of the considered *forcings* as derived from the Trend-Run model. Overall, the annual oscillation (AO) emerges as the most dominant forcing, particularly in the lower stratosphere, where it accounts for over 40% of the variability at approximately 19 km. The semi-annual oscillation (SAO) exhibits its maximum contribution in the troposphere, specifically at 10–11 km. The ENSO forcing displays an absolute maximum contribution of -20% in the lower stratosphere (22–23 km) and has a nearly constant contribution of approximately 10% in the troposphere. The QBO index, obtained for the 70 hPa pressure level, shows almost no contribution in the troposphere and a quasi-constant contribution in the stratosphere ($\sim 4\%$).

Following Fig. 9a, the higher determination coefficient can be observed in the UTLS region (18–20 km), so the higher contribution, in this region, in the trend model is from AO (Fig. 9b). In addition, such a region presents an increase of around 0.25 K per decade (Fig. 8c).

Figure 10 shows temperature trends at the tropopause, CPT (Fig. 10a) and LRT (Fig. 10b) as well as, their standard deviations at the 2σ level (dotted line. So that the standard deviation associated with the trend value corresponds to uncertainty in the trend slope. Temperature at the CPT presents a decreasing trend of $[-0.13 \pm 0.27]$ K per decade,

where seasonal cycles (AO, SAO) seem to be the most dominant forcing Zou et al. (2023), using ERA5 data, observed a tropopause cooling of $[-0.09 \pm 0.03]$ K per decade from 1980 to 2021. Although the time interval (1979–2005) is different from the present study, Tegtmeier et al. (2020) reported a cooling of the tropical CPT from -0.3 to -0.6 K per decade.

On the other hand, LRT temperature (Fig. 10) shows a little insignificant increase ($[0.03 \pm 0.33]$ K per decade), where in the same way as CPT temperature, the seasonal cycles (AO, SAO) are the most dominant forcing. Shang-guan and Wang (2022) and Negash and Raju (2024) also observed a strong influence of AO and SAO in the UT-LS region from COSMIC-1 and ERA-5 data, and COSMIC-1 and Radiosonde data respectively in subtropical latitudes. Following Frierson (2006), the latent heat release caused by thermal forcing in the troposphere is what creates the strong AO in temperature. In addition, according to Loon and Jenne (1969), tropical and sub-tropical SAO are most pronounced in the areas where the Intertropical Convergence Zone crosses the Equator twice a year, in particular, from Eastern Africa to the central Pacific Ocean, which coincides with the region where Réunion is located.

Furthermore, it is important to highlight that the observed trends for both the CPT (cooling) and the LRT (warming) temperatures are directly associated with tropospheric warming, which has been exacerbated by intense accumulation of GHG in the lower troposphere as described by Ladstädter et al. (2023). This phenomenon is a key indicator of climate change and has been observed globally (Ladstädter et al., 2025), reinforcing the intense effect of anthropogenic activities across the planet.

6 Conclusions

Tropopause temperature and height serve as key indicators of anthropogenic climate change, influenced by factors such as stratospheric ozone, greenhouse gas concentrations, and volcanic activity. However, monitoring their variability remains challenging due to the sparse distribution of observation stations, particularly in the Southern Hemisphere. To address this, we compared temperature profiles from three datasets – SHADOZ, COSMIC-1, and MERRA-2 – to assess their similarities and differences and to develop a refined dataset for trend analysis. Our analysis of SHADOZ and COSMIC-1 data (2006–2020) revealed strong agreement in temperature profiles above 10 km. MERRA-2 data showed a good correlation with SHADOZ up to 30 km and with COSMIC-1 above 30 km, but its coarse vertical resolution limited its applicability for tropopause height estimation. Using the Cold Point Tropopause (CPT) and Lapse Rate Tropopause (LRT) methods, we found that CPT-derived tropopause heights and temperatures were consistent across SHADOZ and COSMIC-1, whereas LRT values varied more
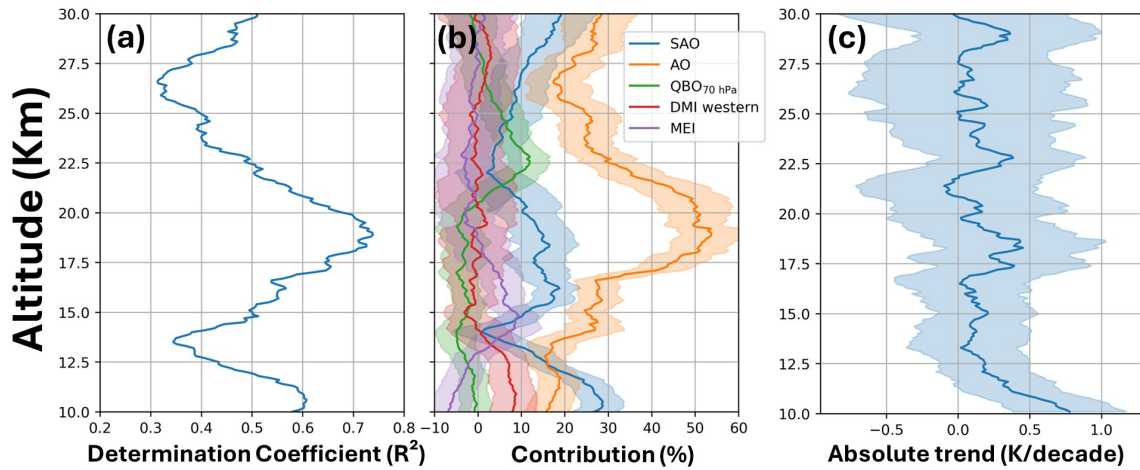
Figure 9. (a) Autocorrelation coefficient profile, **(b)** vertical profile of contribution of each forcing, **(c)** vertical profile of absolute variation of temperature per decade.
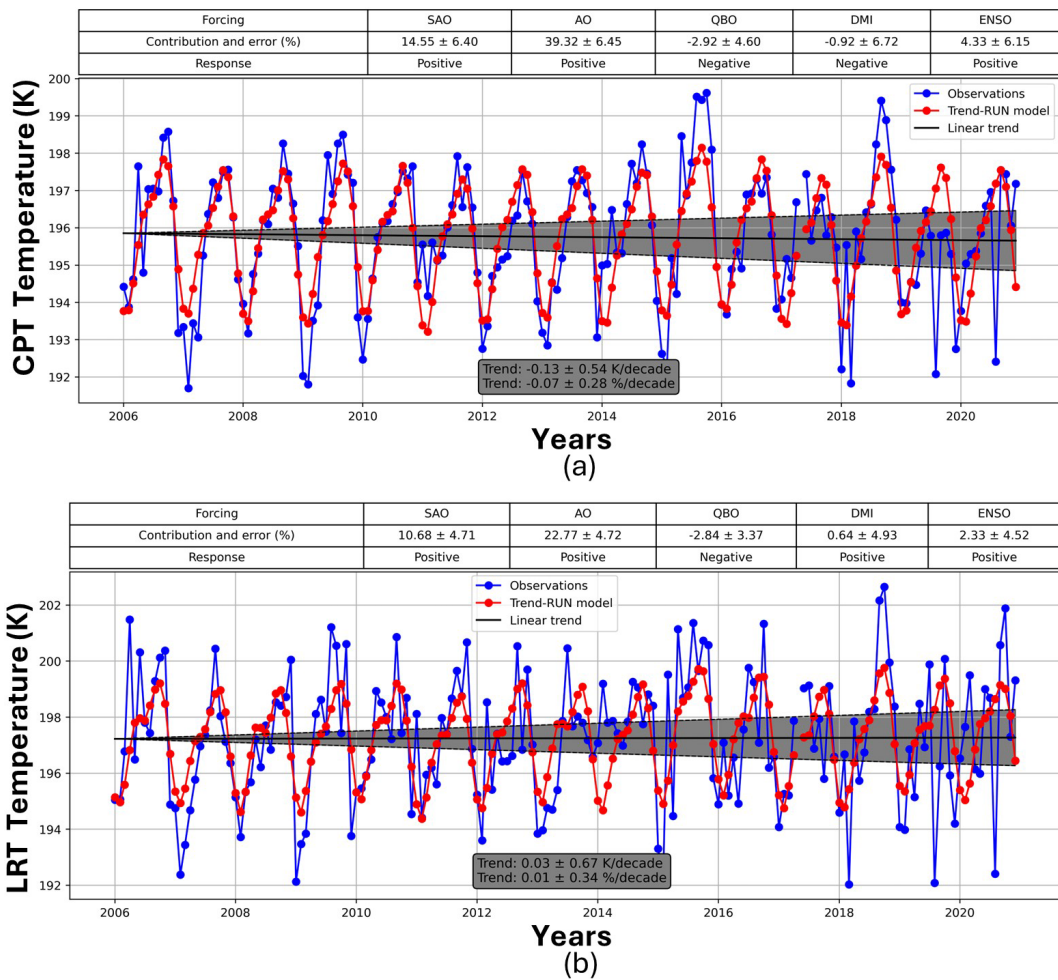
Figure 10. Trend model of CPT **(a)** and LRT **(b)** temperature variation. The black lines represent the trend of CPT and LRT temperature, in figures **(a)** and **(b)**, respectively. The dotted black lines, in both figures, represent the standard deviation of the temperature trend at the 2σ level.

due to differences in vertical resolution. Comparisons within each dataset confirmed that LRT-derived tropopause heights were systematically lower than those from CPT, while LRT temperatures were higher – consistent with previous studies. Additionally, CPT exhibited seasonal variability, with higher values in summer and lower values in winter. To enhance data coverage, we created a new dataset by integrating COSMIC-1 data into SHADOZ profiles between 10 and 30 km, preserving the seasonal characteristics observed in both datasets. This combined dataset improves the representation of tropopause dynamics in regions with sparse observations. Trend analysis highlighted the significant influence of the annual oscillation (AO), particularly in the upper troposphere–lower stratosphere (UT-LS) region. We observed a decreasing trend in CPT temperature (-0.13 ± 0.27 K per decade) and a slightly increasing trend in LRT temperature (0.03 ± 0.33 K per decade), both predominantly influenced by AO and the semi-annual oscillation (SAO). Our findings demonstrate the value of COSMIC-1 data in studying tropopause dynamics, enabling the extension of time series in regions with radiosonde observations and providing critical data where in situ measurements are unavailable. This study underscores the potential of satellite-based remote sensing to enhance our understanding of climate-related changes in the tropopause.

Author contributions. GAM and HB: Conceptualization, Methodology, Software, Analysis, Investigation, Data curation, Visualization, Writing–original draft, Writing and Editing, Funding acquisition, Data Resources and, Supervision. TM: Conceptualization, Methodology, Software, Analysis, Investigation, Data curation, Visualization, Writing–original draft, Writing and Editing. DKP: Conceptualization, Supervision, Analysis, Writing–original draft, Investigation, Writing and Editing, All authors approved the final manuscript.

References

Anthes, R. A., Bernhardt, P. A., Chen, Y., Cucurull, L., Dymond, K. F., Ector, D., Healy, S. B., Ho, S., Hunt, D. C., Kuo, Y., Liu, H., Manning, K., McCormick, C., Meehan, T. K., Randel, W. J., Rocken, C., Schreiner, W. S., Sokolovskiy, S. V., Syndergaard, S., Thompson, D. C., Trenberth, K. E., Wee, T., Yen, N. L., and Zeng, Z.: The COSMIC/FORMOSAT-3 Mission: Early Results, Bulletin of the American Meteorological Society, 89, 313–334, 2008.

Astudillo, J. M., Lau, L., Tang, Y. T., and Moore, T.: A novel approach for the determination of the height of the tropopause from ground-based GNSS observations, Remote Sensing, 12, https://doi.org/10.3390/rs12020293, 2020.

Baldy, S., Ancellet, G., Bessafi, M., Badr, A., and Lan Sun Luk, D.: Field observations of the vertical distribution of tropospheric

ozone at the Island of La Réunion, J. Geophys. Res., 101, 23835–23849, 1996.

Batista, P. P., Clemesha, B. R., and Simonich, D. M.: A 14-year monthly climatology and trend in the 35–65km altitude range from Rayleigh Lidar temperature measurements at a low latitude station, Journal of Atmospheric and Solar-Terrestrial Physics, 71, 1456–1462, 2009.

Bègue, N., Bencherif, H., Sivakumar, V., Kirgis, G., Mze, N., and Leclair de Bellevue, J.: Temperature variability and trends in the UT-LS over a subtropical site: Reunion (20.8° S, 55.5° E), Atmos. Chem. Phys., 10, 8563–8574, https://doi.org/10.5194/acp-10-8563-2010, 2010.

Bencherif, H., Diab, R. D., Portafaix, T., Morel, B., Keckhut, P., and Moorgawa, A.: Temperature climatology and trend estimates in the UTLS region as observed over a southern subtropical site, Durban, South Africa, Atmos. Chem. Phys., 6, 5121–5128, https://doi.org/10.5194/acp-6-5121-2006, 2006.

Birner, T., Sankey, D., and Shepherd, T. G.: The tropopause inversion layer in models and analyses, Geophys. Res. Lett., 33, L14804, https://doi.org/10.1029/2006GL026549, 2006.

Britannica: Réunion, https://www.britannica.com/place/Reunion (last access: 8 May 2025), 2025.

France, J. A., Harvey, V. L., Randall, C. E., Hitchman, M. H., and Schwartz, M. J.: A climatology of stratopause temperature and height in the polar vortex and anticyclones, J. Geophys. Res., 117, D06116, https://doi.org/10.1029/2011JD016893, 2012.

Frierson, D. M.: Robust increases in midlatitude static stability in simulations of global warming, Geophys. Res. Lett., 33, https://doi.org/10.1029/2006GL027504, 2006.

Fueglistaler, S., Dessler, A. E., Dunkerton, T. J., Folkins, I., Fu, Q., and Mote, P. W.: Tropical tropopause layer, Rev. Geophys., 47, RG1004, https://doi.org/10.1029/2008RG000267, 2009.

Global Modeling and Assimilation Office (GMAO): tavg3_3d_asm_Nv: MERRA-2 3D IAU State, Meteorology Instantaneous 3-hourly (p-coord, 0.625x0.5L42), version 5.12.4, Greenbelt, MD, USA: Goddard Space Flight Center Distributed Active Archive Center (GSFC DAAC), https://doi.org/10.5067/SUOQESM06LPK, 2015.

Hoinka, K. P.: Statistics of the Global Tropopause Pressure, Mon. Wea. Rev., 126, 3303–3325, 1998.

Ladstädter, F., Steiner, A. K., and Gleisner, H.: Resolving the 21st century temperature trends of the upper troposphere–lower stratosphere with satellite observations, Sci. Rep. 13, 1306, https://doi.org/10.1038/s41598-023-28222-x, 2023.

Ladstädter, F., Stocker, M., Scher, S., and Steiner, A. K.: Observed changes in the temperature and height of the globally resolved lapserate tropopause, Atmos. Chem. Phys., 25, 16053–16062, https://doi.org/10.5194/acp-25-16053-2025, 2025.

Loon, H. V. and Jenne, R. L.: The Half-Yearly Oscillations in the Tropics of the Southern Hemisphere, J. Atmos. Sci., 26, 218–232, 1969.

Morioka, Y., Tozuka, T., and Yamagata, T.: Climate variability in the southern Indian Ocean as revealed by self-organizing maps, Clim. Dyn., 35, 1059–1072, 2010.

NASA Goddard Space Flight Center (GSFC) SHADOZ Team: Southern Hemisphere ADditional OZonesondes (SHADOZ) Version 06 (V06) Station Data (Version V06), NASA

[SHADOZ] [data set], https://doi.org/10.57721/SHADOZ-V06, 2019.

Negash, T. and Raju, U. P.: Study on long term troposphere lower stratosphere temperature (TLST) trend in tropical and subtropical northern hemisphere using ground based and COSMIC satellite data, Journal of Atmospheric and Solar-Terrestrial Physics, 261, 106306, https://doi.org/10.1016/j.jastp.2024.106306, 2024.

Randel, W. and Jensen, E.: Physical processes in the tropical tropopause layer and their roles in a changing climate, Nature Geosci., 6, 169–176, 2013.

Randel, W. J. and Cobb, J. B.: Coherent variations of monthly mean total ozone and lower stratospheric temperature, J. Geophys. Res., 99, 5433–5447, 1994.

Randel, W. J., Wu, F., and Gaffen, D. J.: Interannual variability of the tropical tropopause derived from radiosonde data and NCEP reanalyses, J. Geophys. Res, 105 , 15509–15523, 2000.

Reid, G. C. and Gage, K. S.: On the annual variation in height of the tropical tropopause, J. Atmos. Sci., 38, 1928–1938, 1981.

Reid, G. C. and Gage, K. S.: A relationship between the height of the tropical tropopause and the global angular momentum of the atmosphere, Geophys. Res. Lett., 1, 840–842, 1984.

Reid, G. C. and Gage, K. S.: Interannual variations in the height of the tropical tropopause, J. Geophys. Res., 90, 5629–5635, 1985.

Saji, N. H., Goswami, B. N., Vinayachandran, P. N., and Yamagata, T.: A dipole mode in the tropical Indian Ocean, Nature 401, 360–363, 1999.

Santer, B. D., L. Wigley, T. M., Simmons, A. J., Kållberg, P. W., Kelly, G. A., Uppala, S. M., Ammann, C., Boyle, J. S., Brüggemann, W., Doutriaux, C., Fiorino, M., Mears, C., Meehl, G. A., Sausen, R., Taylor, K. E., Washington, W. M., Wehner, M. F., and Wentz, F. J.: Identification of anthropogenic climate change using a second-generation reanalysis, J. Geophys. Res., 109, D21104, https://doi.org/10.1029/2004JD005075, 2004.

Schmidt, T., Wickert, J., Beyerle, G., and Reigber, C.: Tropical tropopause parameters derived from GPS radio occultation measurements with CHAMP, J. Geophys. Res., 109, D13105, https://doi.org/10.1029/2004JD004566, 2004.

Seidel, D. J., Ross, R. J., and Angell, J. K.: Climatological characteristics of the tropical tropopause as revealed by radiosonde, J. Geophys. Res., 106, 7857–7878, 2001.

Selkirk, H. B.: The tropopause cold trap in the Australian monsoon during STEP/AMEX 1987, J. Geophys. Res., 98, 8591–8610, 1993.

Shangguan, M. and Wang, W.: The semi-annual oscillation (SAO) in the upper troposphere and lower stratosphere (UTLS), Atmos. Chem. Phys., 22, 9499–9511, https://doi.org/10.5194/acp-22-9499-2022, 2022.

Sivakumar, V., Baray, J.-L., Baldy, S., and Bencherif, H.: Tropopause characteristics over a southern subtropical site, Reunion Island (21° S, 55° E): Using radiosonde–ozonesonde data, J. Geophys. Res., 111, D19111, https://doi.org/10.1029/2005JD006430, 2006.

Sivakumar, V., Bencherif, H., Bègue, N., and Thompson, A. M.: Tropopause Characteristics and Variability from 11 yr of SHADOZ Observations in the Southern Tropics and Subtropics, J. Appl. Meteor. Climatol., 50, 1403–1416, 2011a.

Sivakumar, V., Vishnu Prasanth, P., Kishore, P., Bencherif, H., and Keckhut, P.: Rayleigh LIDAR and satellite (HALOE, SABER, CHAMP and COSMIC) measurements of stratosphere-

mesosphere temperature over a southern sub-tropical site, Reunion (20.8° S; 55.5° E): climatology and comparison study, Ann. Geophys., 29, 649–662, 2011b.

Sivakumar, V., Jimmy, R., Bencherif, H., Bègue, N., and Portafaix, T.: Use of the TREND RUN model to deduce trends in South African Weather Service (SAWS) atmospheric data: Case study over Addo (33.568° S, 25.692° E) Eastern Cape, South Africa, Journal of Neutral Atmosphere, 51–58, hal-02098051, 2017.

Sterling, C. W., Johnson, B. J., Oltmans, S. J., Smit, H. G. J., Jordan, A. F., Cullis, P. D., Hall, E. G., Thompson, A. M., and Witte, J. C.: Homogenizing and estimating the uncertainty in NOAA's long-term vertical ozone profile records measured with the electrochemical concentration cell ozonesonde, Atmos. Meas. Tech., 11, 3661–3687, https://doi.org/10.5194/amt-11-3661-2018, 2018.

Tegtmeier, S., Anstey, J., Davis, S., Dragani, R., Harada, Y., Ivanciu, I., Pilch Kedzierski, R., Krüger, K., Legras, B., Long, C., Wang, J. S., Wargan, K., and Wright, J. S.: Temperature and tropopause characteristics from reanalyses data in the tropical tropopause layer, Atmos. Chem. Phys., 20, 753–770, https://doi.org/10.5194/acp-20-753-2020, 2020.

Toihir, A. M., Portafaix, T., Sivakumar, V., Bencherif, H., Pazmiño, A., and Bègue, N.: Variability and trend in ozone over the southern tropics and subtropics, Ann. Geophys., 36, 381–404, 2018.

Thompson, A. M., Witte, J. C., McPeters, R. D., Oltmans, S. J., Schmidlin, F. J., Logan, J. A., Fujiwara, M., H. Kirchhoff, W. J., Posny, F., R. Coetzee, G. J., Hoegger, B., Kawakami, S., Ogawa, T., Johnson, B. J., Vömel, H., and Labow, G.: Southern Hemisphere Additional Ozonesondes (SHADOZ) 1998–2000 tropical ozone climatology 1. Comparison with Total Ozone Mapping Spectrometer (TOMS) and ground-based measurements, J. Geophys. Res., 108, 8238, https://doi.org/10.1029/2001JD000967, 2003.

Thompson, A. M., Witte, J. C., Sterling, C., Jordan, A., Johnson, B. J., Oltmans, S. J., Fujiwara, M., Vömel, H., Allaart, M., Piters, A., R. Coetzee, G. J., Posny, F., Corrales, E., Diaz, J. A., Félix, C., Komala, N., Lai, N., Ahn Nguyen, H. T., Maata, M., et al.: First reprocessing of Southern Hemisphere Additional Ozonesondes (SHADOZ) ozone profiles (1998–2016): 2. Comparisons with satellites and ground-based instruments, Journal of Geophysical Research: Atmospheres, 122, 13000–13025, https://doi.org/10.1002/2017JD027406, 2017.

Thompson, A. M., Stauffer, R. M., Wargan, K., Witte, J. C., Kollonige, D. E., and Ziemke, J. R.: Regional and seasonal trends in tropical ozone from SHADOZ profiles: Reference for models and satellite products, J. of Geophys. Res. Atmos., 126, https://doi.org/10.1029/2021JD034691, 2021.

UCAR COSMIC Program: COSMIC-1 Data Products, UCAR/NCAR – COSMIC [data set], https://doi.org/10.5065/ZD80-KD74, 2002.

Vignon, E. and Mitchell, D. M.: The stratopause evolution during different types of sudden stratospheric warming event, Clim. Dyn., 44, 3323–3337, 2015.

Witte, J. C., Thompson, A. M., Smit, H. G. J., Fujiwara, M., Posny, F., Coetzee, G. J. R., Northam, E. T., Johnson, B. J., Sterling, C. W., Mohamad, M., Ogino, Shin-Ya, Jordan, A., and da Silva, F.: First reprocessing of Southern Hemisphere ADditional OZonesondes (SHADOZ) profile records (1998-2015): 1. Methodology and evaluation, J. Geophys. Res. Atmos., 122, 6611–6636, 2017.

Witte, J. C., Thompson, A. M., Smit, H. G. J., Vömel, H., Posny, F., and Stübi, R.: First reprocessing of Southern Hemisphere ADditional OZonesondes profile records: 3. Uncertainty in ozone profile and total column, Journal of Geophysical Research: Atmospheres, 123, 3243–3268, https://doi.org/10.1002/2017JD027791, 2018.

WMO: Definition of the tropopause, WMO Bull., 6, 136, 1957.

Xia, P., Shan, Y., Ye, S., and Jiang, W.: Identification of Tropopause Height with Atmospheric Refractivity, J. Atmos. Sci., 78, 3–16, 2021.

Xian, T. and Homeyer, C. R.: Global tropopause altitudes in radiosondes and reanalyses, Atmos. Chem. Phys., 19, 5661–5678, https://doi.org/10.5194/acp-19-5661-2019, 2019.

Zhran, M. and Mousa, A.: Global tropopause height determination using GNSS radio occultation, The Egyptian Journal of Remote Sensing and Space Science, 26, 317–331, 2023.

Zhran, M., Mousa, A., Alshehri, F., and Jin, S.: Evaluation of Tropopause Height from Sentinel-6 GNSS Radio Occultation Using Different Methods, Remote Sens., 15, 5513, https://doi.org/10.3390/rs15235513, 2023.

Zou, L., Hoffmann, L., Müller, R., and Spang, R.: Variability and trends of the tropical tropopause derived from a 1980–2021 multi-reanalysis assessment, Front. Earth Sci., 11, 1177502, https://doi.org/10.3389/feart.2023.1177502, 2023.